The ISME Journal (2007) 1, 354–360

www.nature.com/ismej

ORIGINAL ARTICLE

Carbon and nitrogen fixation and metabolite exchange in and between individual cells of *Anabaena oscillarioides*

Radu Popa[1], Peter K Weber[2], Jennifer Pett-Ridge[2], Juliette A Finzi[3], Stewart J Fallon[2], Ian D Hutcheon[2], Kenneth H Nealson[2] and Douglas G Capone[3]

[1]*Department of Biology, Portland State University, Portland, OR, USA;* [2]*Glenn T. Seaborg Institute, Chemistry, Materials and Life Sciences Directorate, Lawrence Livermore National Laboratory, Livermore, CA, USA and* [3]*Department of Biological Sciences, University of Southern California, Los Angeles, CA, USA*

Filamentous nitrogen fixing cyanobacteria are key players in global nutrient cycling, but the relationship between CO_2- and N_2-fixation and intercellular exchange of these elements remains poorly understood in many genera. Using high-resolution nanometer-scale secondary ion mass spectrometry (NanoSIMS) in conjunction with enriched $H^{13}CO_3^-$ and $^{15}N_2$ incubations of *Anabaena oscillarioides*, we imaged the cellular distributions of C, N and P and ^{13}C and ^{15}N enrichments at multiple time points during a diurnal cycle as proxies for C and N assimilation. The temporal and spatial distributions of the newly fixed C and N were highly heterogeneous at both the intra- and inter-cellular scale, and indicative of regions performing active assimilation and biosynthesis. Subcellular components such as the neck region of heterocycts, cell division septae and putative cyanophycin granules were clearly identifiable by their elemental composition. Newly fixed nitrogen was rapidly exported from heterocysts and was evenly allocated among vegetative cells, with the exception of the most remote vegetative cells between heterocysts, which were N limited based on lower ^{15}N enrichment. Preexisting functional heterocysts had the lowest levels of ^{13}C and ^{15}N enrichment, while heterocysts that were inferred to have differentiated during the experiment had higher levels of enrichment. This innovative approach, combining stable isotope labeling and NanoSIMS elemental and isotopic imaging, allows characterization of cellular development (division, heterocyst differentiation), changes in individual cell composition and cellular roles in metabolite exchange.

The ISME Journal (2007) **1,** 354–360; doi:10.1038/ismej.2007.44; published online 5 July 2007
Subject Category: geomicrobiology and microbiol contributions to geochemical cycles
Keywords: cyanobacteria; heterocyst; nitrogen fixation; nitrogenase; *Anabaena*

Introduction

Some cyanobacteria are uniquely capable of fixing both dinitrogen (N_2) and carbon dioxide (CO_2), deriving energy from oxygenic photosynthesis. These capabilities and the abundance of cyanobacteria in phytoplankton communities make these microorganisms keystone species in the global biogeochemical cycles of carbon and nitrogen. Under conditions of N limitation, some vegetative cells of *Anabaena oscillarioides* (a filamentous freshwater cyanobacterium) differentiate to form heterocysts non-growing, specialized cells in which N_2 is fixed into organic N (Stewart, 1973; Herrero *et al.*, 1979; Kumar *et al.*, 1983; Wolk, 1996, 2000; Meeks and Elhai, 2002). Because the enzyme that catalyzes N_2 fixation, nitrogenase, is inhibited by oxygen (Stewart, 1973; Gotto *et al.*, 1979; Smith *et al.*, 1987), heterocysts must be physically isolated from nearby vegetative cells, which are sites of oxygenic photosynthesis and CO_2-fixation. This isolation, however, cannot be complete, as vegetative and heterocyst cells must exchange energy, organic C and fixed N (Figure 1). How these two cell types coexist in the same filament, managing to share resources and maintain equilibrium between oxygenic photosynthesis and N_2-fixation, remains poorly understood.

This apparent conundrum, that is the juxtaposition of oxygen-sensitive functions with oxygen-producing cells, has long been a focus of cyanobacterial biology, and a variety of experimental approaches have been used to decipher the functional and

Correspondence: Professor DG Capone, Department of Biological Sciences, University of Southern California, 3616, Trousdale Parkway, USC, Los Angeles, CA 90089-0740, USA.
E-mail: capone@usc.edu
Received 5 April 2007; revised 14 May 2007; accepted 14 May 2007; published online 5 July 2007

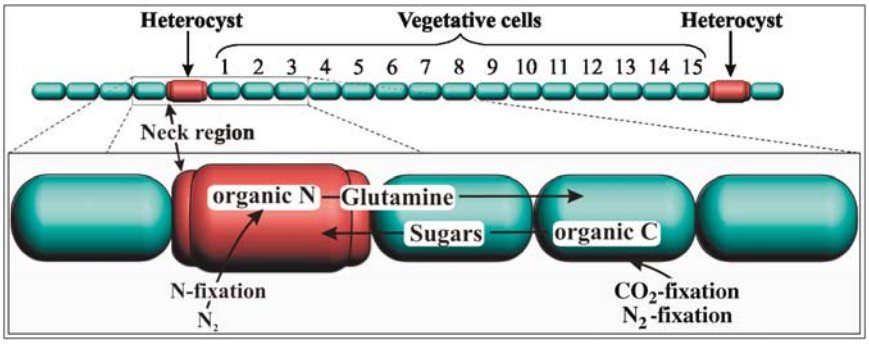

Figure 1 Model of CO_2- and N_2-fixation and transport in a filament of *A. oscillarioides* showing two heterocysts. The numbers indicate vegetative cells at different distances from the heterocysts.

physiological differences between heterocysts and vegetative cells (Thomas *et al.*, 1975, 1977; Wolk *et al.*, 1976; Meeks *et al.*, 1977; Kumar *et al.*, 1983; Flores *et al.*, 2006). Pulse–chase experiments and autoradiography using the short-lived radioisotope ^{13}N have demonstrated that heterocysts are the site of N_2-fixation and showed both incorporation of N_2 by heterocyst and export of recently fixed organic N to vegetative cells (Wolk *et al.*, 1974). Isotope labeling with ^{14}C has been used to demonstrate photosynthesis in vegetative cells and the subsequent movement of this C into heterocysts (Wolk, 1968). Finally, labeling of RNA and proteins with fluorescent probes, as well as immunolocalization experiments, has revealed the differential distribution and expression of various biomolecules (including nitrogenase and RuBisCO) in both heterocysts and vegetative cells (Murry *et al.*, 1984). Hence, discrete processes occur within, and a rapid exchange of organic materials occurs between, heterocysts and vegetative cells (Wolk *et al.*, 1976; Meeks and Elhai, 2002; Flores *et al.*, 2006). However, much remains to be learned about the dynamics of CO_2- and N_2-fixation in filamentous cyanobacteria, particularly the synchronization, mobilization and exchange of C and N among cells (Flores *et al.*, 2006). To study these phenomena, the ability to analyze metabolite exchange between microbial cells and assess physiological performance at the single cell level is critical.

Our objective was to characterize the patterns of uptake and exchange of metabolites by *A. oscillarioides*' two morphologically and functionally distinct cell types. We used tracer-level additions of inorganic ^{13}C and ^{15}N, and tracked these stable isotopes from inorganic pools to their cellular fate by imaging with high-resolution nanometer-scale secondary ion mass spectrometry (NanoSIMS). NanoSIMS provides the ability to map distributions of elements and isotopes with 50–100 nm resolution (Lechene *et al.*, 2006). This approach allowed measurement of C and N uptake and subsequent distribution at the cellular and subcellular level.

Materials and methods

A. oscillarioides was grown in liquid culture at room temperature with continual aeration at pH ~ 7.5 with 4.5 mM $NaHCO_3/Na_2CO_3$ buffer, 240 μM $CaCl_2$, 60 μM K_2HPO_4, 100 μM $MgSO_4$, 5 μM EDTA, 8 μM Fe^{3+} and 1% Walsby trace elements mixture (Walsby, 1972). For the tracer uptake experiment, exponential-phase cultures were transferred to 162 ml serum vials with crimp-seal silicone rubber closures and without a gas phase.

Incubations were started 2 h after the beginning of the light cycle with a 12 h light:12 h dark illumination regime, using visible light with an irradiance of ~20 μmol quanta $m^{-2}\,s^{-1}$. We initiated incubation by injecting 0.07 ml of $NaH^{13}CO_3$ (~99 atm% ^{13}C, 0.047 M) (Cambridge Isotope Laboratories Inc., Cambridge, MA, USA) to reach a final enrichment of 1.7 atm% ^{13}C-DIC and 0.3 ml of 99% $^{15}N_2$ (Isotec, Sigma-Aldrich, St Louis, MO, USA) to reach 0.57 mM N_2 (13.6% ^{15}N). A vial was destructively sampled at each interval ($T0 = 0$ min (control), $T1 = 15$ min, $T2 = 30$ min, $T3 = 1$ h, $T4 = 2$ h, $T5 = 4$ h, $T6 = 8$ h and $T7 = 24$ h), and cells were fixed with 2% glutaraldehyde (EM Science, Gibbstown, NJ, USA). Thus the 24 h sample experienced 8 h of light, 12 h of dark and 2 additional hours of light.

Before NanoSIMS microanalysis, the filaments of *A. oscillarioides* were filtered, washed with Milli-Q (18 MΩ) H_2O and transferred onto a silica chip and dried. NanoSIMS (Cameca, Gennevilliers Cedex, France) was performed at Lawrence Livermore National Laboratory (LLNL) using a Cameca NanoSIMS 50 instrument. An ~2 pA Cs^+ primary beam was focused to a nominal spot size of ~100 nm and stepped over the sample in a 256 × 256 pixel raster to generate secondary ions. Dwell time was 1 ms/pixel, and raster size was 5–10 μm^2. The secondary mass spectrometer was tuned for ~6800 mass resolving power to resolve isobaric interferences. Five secondary ions ($^{12}C^-$, $^{13}C^-$, $^{12}C^{14}N^-$, $^{12}C^{15}N^-$ and $^{31}P^-$) were detected in simultaneous collection mode by pulse counting to generate 10–20 serial quantitative secondary ion images (that is, layers). Samples

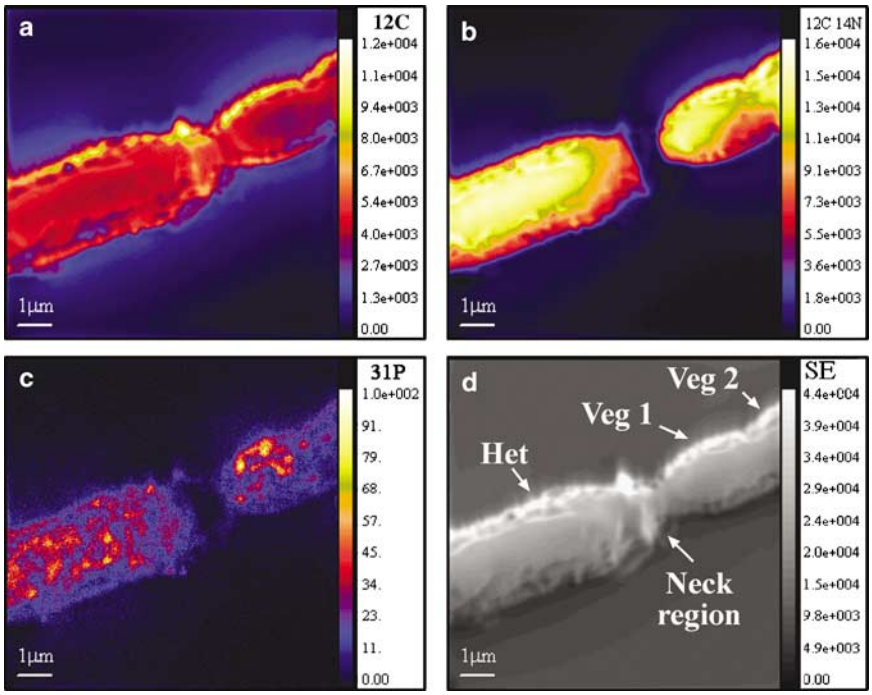

Figure 2 NanoSIMS (**a**) carbon, (**b**) nitrogen (as CN), (**c**) phosphorus and (**d**) secondary electron (SE) images of a segment from a filament of *A. oscillarioides* showing part of a heterocyst (Het), a vegetative cell (Veg 1) and part of a second vegetative cell (Veg 2). The neck region of the heterocyst is distinguished by the low abundance of P and N. The color bars indicate the number of ions or electrons collected per pixel.

were also imaged simultaneously by secondary electrons. Samples were presputtered to a depth of ~100 nm before measurements to achieve sputtering equilibrium. The depth of analysis during a measurement was between 50 and 200 nm. For each time point, several different filaments were analyzed, and measurements were repeated on selected cells to ensure measurement accuracy. Selected samples were also sputtered at high beam currents (~1 nA) between repeat measurements to determine if isotopic composition changed; no significant changes were found with cell depth.

Data were processed as quantitative isotopic ratio images using custom software, and were corrected for detector dead time and image shift from layer to layer. Each cell was defined as a region of interest (ROI), and the isotopic composition for each ROI was calculated by averaging over all of the replicate layers. Finely, ground bovine liver sample (NIST SRM 1577b) was used as a reference standard for the C and N isotopic measurements ($^{13}C/^{12}C = 0.0110$; $^{15}N/^{14}N = 0.00370$; results of inter-lab round robin, reported by William Mark, Environmental Isotope Lab, University of Waterloo, private communication, March 2004). Measurement precision, $\sigma_{(\text{internal})}$, was 0.4–1.4% ($2\sigma$) for individual $^{13}C/^{12}C$ and $^{15}N/^{15}N$ measurements, and replicate analyses of the standard yielded an analytical precision, $\sigma_{(\text{std})}$, of 2.1% (2σ) for an individual measurement. Precision for replicate analyses, $\sigma_{(\text{external})}$, was calculated by summing in quadrature the standard error of the mean of the analyses, $\sigma_{(\text{internal})}$, with the limit of analytical precision for the number of measurements performed,

$$(\sigma_{(\text{std})}/\sqrt{n}) : \sigma_{(\text{external})_c} = \sqrt{\sigma^2_{(\text{internal})} + (\sigma_{(\text{std})}/\sqrt{n})^2} \quad (1)$$

Summary data (Figure 3) are presented as atom percent excess (APE) to provide the reader with a clear understanding of the uptake of the stable isotope tracers. APE was calculated based on the initial isotopic ratios of the organism at $T = 0$ (R_i) and the isotopic ratio of the sampled organism (R_f):

$$\text{APE} = [R_f/(R_f + 1) - R_i/(R_i + 1)]100\% \quad (2)$$

Data (Figure 3) are also presented as net fixation (Fx_{net}), the percentage of C or N incorporated into the organism relative to the initial C or N content, respectively:

$$\text{Fx}_{\text{net}} = F_s/F_i \times 100\%, \quad (3)$$

where F_i is the fraction of C or N in the sampled organism from the initial C or N content of the organism and F_s is the fraction of C or N in the sampled organism taken up from the spiked HCO_3^- or N_2 pools. F_i and F_s are derived from a two component mixing model:

$$F_{\text{minor}} = F_i\,[R_i/(R_i + 1)] + F_s\,[R_s/(R_s + 1)] \text{ and} \quad (4)$$

$$F_{\text{major}} = F_i\,[1/(R_i + 1)] + F_s\,[1/(R_s + 1)] \quad (5)$$

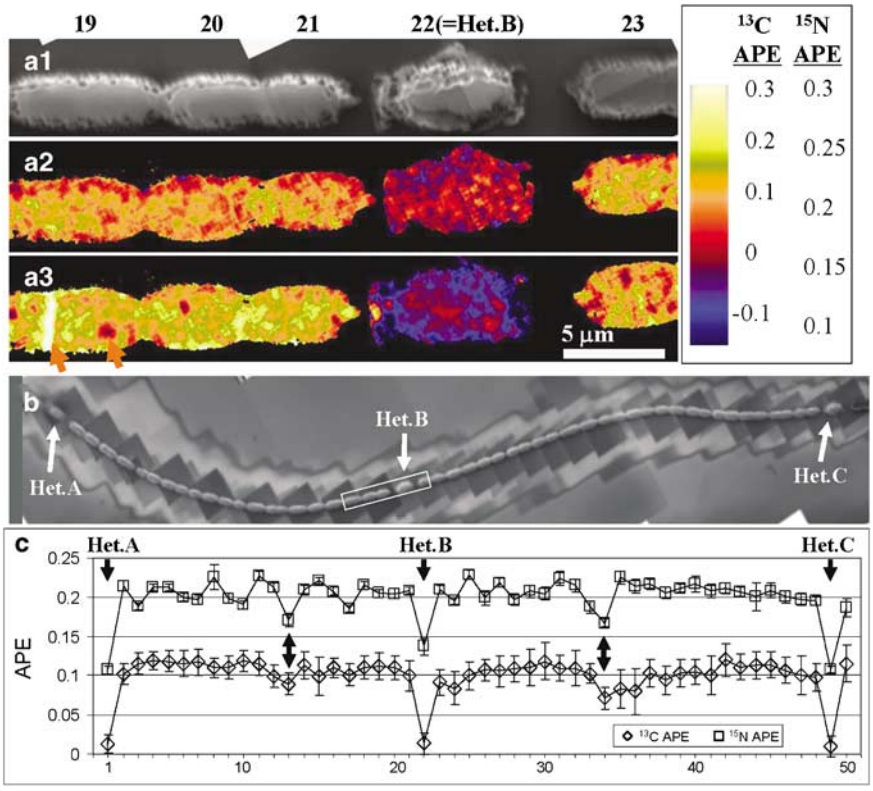

Figure 3 (**a**) Chain of five cells from a filament of *A. oscillarioides* analyzed with NanoSIMS after 4 h of incubation with $H^{13}CO_3^-$ and $^{15}N_2$. Het = Heterocyst. Individual cells are numbered to correspond with the numbering in (**c**). (a1) Image reconstruction based on secondary electrons. (a2) The distribution of ^{13}C enrichment. (a3) The distribution of ^{15}N enrichment. Enrichment is expressed as atom percent enrichment (APE). (**b**) Post-analysis NanoSIMS secondary electron image of a filament of 50 cells of *A. oscillarioides* showing three heterocysts (Het) after 4 h of incubation with $H^{13}CO_3^-$ and $^{15}N_2$. The white box indicates the area shown in the images a1, a2 and a3. (**c**) The cell-to-cell variation in ^{13}C (diamonds) and ^{15}N enrichment (squares) along the same 50 cells filament. There are 1–6 independent replicate measurements per cell. Error bars represent two standard errors.

where F_{minor} and F_{major} are the final atomic fractions of the minor and major isotope in the sampled organism, and R_i and R_s are the isotopic ratios in the initial and spiked pools, respectively. Fx_{net} is calculated by taking the ratio of equations (4) and (5), which is equal to the final isotopic ratio in the sampled organism, R_f, solving for F_s/F_i, and substituting the result into equation (3):

$$\begin{aligned} \mathrm{Fx_{net}} = &\{R_f[1 - R_i/(R_i + 1)] \\ &- R_i/(R_i + 1)\}/\{R_s/(R_s + 1) \\ &- R_f[R_s/(R_s + 1)]\} \times 100\%. \end{aligned} \quad (6)$$

For each time point, a sample of bulk cell biomass was also analyzed by isotope ratio mass spectrometry to determine average APE and net-fixation values. Each sample was filtered onto pre-combusted GF/F filters and dried. Samples were analyzed at the USC Stable Isotope Facility on a VG IsoPrime interfaced to an elemental analyzer run in continuous-flow mode.

Results and discussion

In the NanoSIMS images, mature heterocysts of *A. oscillarioides* are distinguishable from the vegetative cells based on size, shape, and intercellular distances (Figure 2). The neck region of the heterocyst are easily identified in the NanoSIMS images because they are enriched in polysaccharides and therefore low in P and N. Desiccation of the filaments on the silicon wafers results in changes in size of the cells and, in some cases, separation of the vegetative cells from the heterocyst neck region (Figure 3). Cell-average enrichment data are extracted based on the cell images (Figures 3 and 4).

Intracellular isotopic heterogeneity can be resolved in the NanoSIMS images. For example, the highly ^{15}N-enriched region dividing the elongated cell #19 from Figure 3a3 probably represents a cell division plane. Similar features are observed in other cells. Although the various division stages have already been identified in cyanobacterial cells (Mazouni *et al.*, 2004; Klint *et al.*, 2007), the connection with the relative biosynthetic age of the participating proteins has been more difficult to make. We presume that the zone in this and other similar cells are enriched in ^{15}N because cell division includes the formation of a scaffold and septum (deBoer *et al.*, 1992; Erickson, 1997; Ghigo and Beckwith, 2000) composed of newly formed proteins and newly diaminated amino acids. These

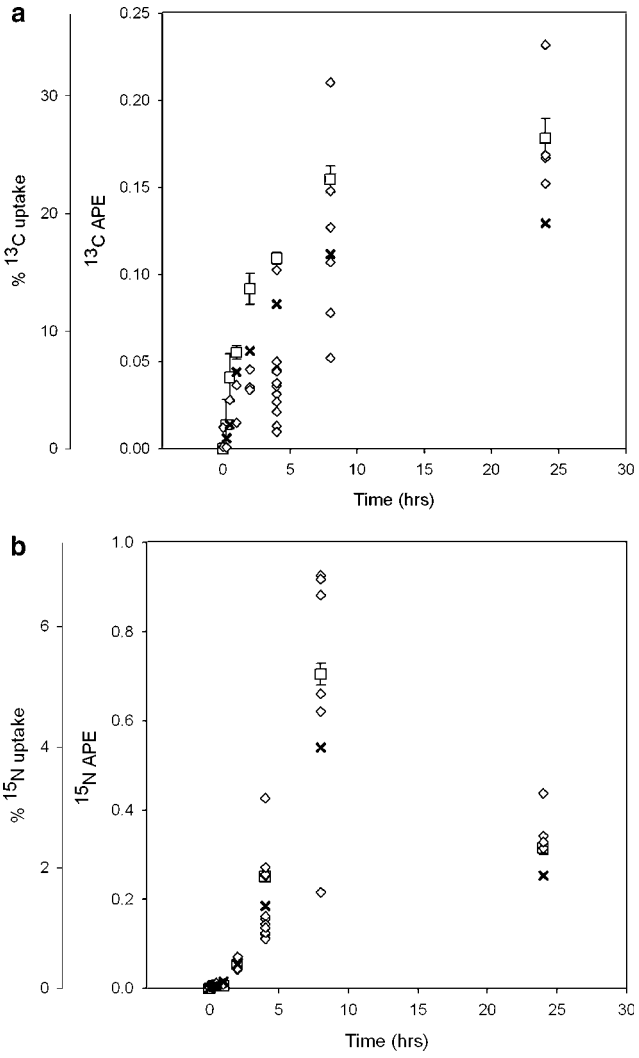

Figure 4 Atom percent enrichment (APE) for (**a**) ^{13}C and (**b**) ^{15}N and calculated C and N net fixation by *A. oscillarioides* against incubation time for heterocysts (squares) and vegetative cells (diamonds) as determined by NanoSIMS imaging, compared to bulk (from isotope ratio mass spectrometry) sample data (**X**). Data from 2 to 12 individual cells per time point are plotted for heterocysts; average data are plotted for vegetative cells (average $n = 25$ cells per time point). Two sigma error bars are present but largely smaller than the data points.

zones have no significant parallel enrichment in ^{13}C in the separating wall/septum (Figure 3a2). The elevated ^{15}N in the septum shows the contribution of newly fixed N to cell division and implies the incorporation of amino acids carrying newly fixed N before and during cell division. The absence of ^{13}C enrichment in the surrounding cellular material indicates that the septum proteins are made from a ^{13}C-averaged pool of amino acid scaffolds, whereas the N used in the amination of some of these amino acids is fixed recently (<4 h).

Vegetative cells also have subcellular circular zones that are isotopically distinct in ^{15}N relative to the cell mass (Figure 3). Zones that are less enriched in ^{15}N likely have a pre-experiment origin (one ^{15}N-poor zone is indicated in Figure 3a3 cell #19); those that are highly enriched in ^{15}N are composed of newly fixed N. These zones are likely cyanophycin granules, a polymer of asparagine and aspartate that *A. oscillarioides* uses for N storage (Simon, 1987). Positive identification of subcellular structures could be performed using histological analysis before NanoSIMS analysis (Simon, 1987).

The rate of CO_2- and N_2-fixation and the fate of recently fixed C and N can be determined based on ^{13}C and ^{15}N enrichment of the cells over time. For example, after 4 h of incubation, vegetative cells exhibit significant enrichment in both ^{13}C and ^{15}N because of active CO_2- and N_2-fixation and intercellular exchange (Figure 3). CO_2-fixation initiates rapidly in the photoperiod, reaching 13.6% net fixation after only 2 h, and slows down in the later photoperiod, ending with 28.1% net fixation (Figure 4a). In contrast, N_2-fixation starts slowly (0.4% net fixation at 2 h) and increases significantly after 4 h of light, reaching a maximum of 5.3% net fixation after 8 h of incubation (Figure 4b). Bulk isotopic analyses for the same samples show the same general pattern, with some slight differences in the absolute mean isotopic composition, which may be a result of the method of averaging across the cells from the NanoSIMS analysis (see Materials and methods).

During the photosynthetic period (first 8 h of our experiment), more of the newly fixed C (indicated by ^{13}C enrichment) is allocated to vegetative cells than to heterocysts (Figures 3a2, 3c and 4a). This is consistent with earlier work (Wolk, 1968) and is likely a result of high growth and cell division rates, and thus higher C requirements, in vegetative cells. In contrast, mature heterocysts are non-growing cells and thus after differentiation and maturation ends, they have little need for biosynthetic materials. The primary carbon requirements of heterocysts are for energy and reducing power to support N_2-fixation, and synthesis of C skeletons used in the production of the amino acids that export N to vegetative cells. Because heterocysts do not have a functional photosystem II, they rely on vegetative cells for their reduced C needs.

A possibly counterintuitive result, but also consistent with earlier work, is that levels of newly fixed N (^{15}N-enrichment) are higher in vegetative cells than in mature heterocysts (Figures 3a3, 3c and 4b). These heterocysts exhibit markedly lower ^{13}C enrichment as well (indicating their genesis occurred before this experiment) and are thus easily identified. This result indicates a very rapid export of organic N from heterocysts to vegetative cells, keeping pace with the N demands of vegetative cells in the first hours of the day, driven by their active growth and cell division. Indeed, using the short-lived radioisotope ^{13}N, Wolk *et al.* (1974, 1976) demonstrated that heterocysts of *A. variabilis* fix N_2- and distribute it very quickly (<1.5 min) to vegetative cells. Our data indicate that this rapid

redistribution of newly fixed N compounds persists throughout the daylight period.

The NanoSIMS data show how N transport and limitation are related to heterocyst differentiation (Figure 3c). During the growth of *A. oscillarioides*, the number of vegetative cells between two heterocysts progressively increases with vegetative cell division, and when this number exceeds a threshold, a vegetative cell situated approximately halfway between two heterocysts differentiates into a new heterocyst (Wolk, 2000; Mazouni *et al.*, 2004). At the organism level, it is the overall N deprivation of filaments that induces heterocyst differentiation (deBoer *et al.*, 1992; Klint *et al.*, 2007). Therefore, it is logical to assume that vegetative cells more remote from the nearest heterocyst would experience a higher degree of N limitation and would be induced to initiate heterocyst differentiation. The NanoSIMS ^{15}N-enrichment data show that rather than a gradient of N limitation from the heterocysts to the vegetative cells near the midpoint between extant heterocysts, N availability is only limited at the midpoint ($\sim$8–12 cells apart; Figure 3c). The observed variability in ^{15}N enrichment in vegetative cells is likely the result of differences in the life stage of, and the heterogeneity of N storage within, individual cells. The ^{13}C enrichment profiles across contiguous filaments of vegetative cells are relatively flat, showing that N limitation is not limiting CO_2-fixation and use at more remote vegetative cells (Figure 3c). The midpoint cells appear slightly less enriched in ^{13}C, suggesting they have slowed or ceased photosynthesis, and may be about to initiate the process of heterocyst formation in which they will differentiate into proheterocysts and later into mature heterocysts (Wolk, 2000; Mazouni *et al.*, 2004). The lack of N and C gradients in the vegetative cells suggests that N transport among vegetative cells is very rapid relative to use, and that heterocyst differentiation is signaled by N limitation at the scale of one to three cells.

The patterns of isotopic enrichment over time for vegetative cells and heterocysts reflect cell physiology and development. While ^{13}C and ^{15}N enrichment for the vegetative cells increases progressively and is relatively uniform during the light period of the experiment, the enrichment data for the heterocysts diverge significantly with time. Some heterocysts become more enriched while others are more depleted in ^{13}C and ^{15}N relative to the vegetative cells (Figure 4). Heterocysts that are substantially enriched in ^{13}C and ^{15}N are most likely those that have recently differentiated, because in this process, newly fixed C and N are used to synthesize the new biomachinery required for N_2 fixation. We presume that heterocysts with substantially lower ^{13}C and ^{15}N enrichment have differentiated before the introduction of the isotopic label and are still functional (still fixing N) because adjacent vegetative cells exhibit ^{15}N enrichment. After a one-day cycle, which included a dark period, the ^{13}C and ^{15}N enrichment of heterocysts is less heterogeneous; this indicates that pre-existing heterocysts have performed repair with newly fixed N and C, elevating their isotopic composition to a level close to that of the newly differentiated heterocysts. We speculate that the relative decrease in ^{15}N enrichment in the 24 h sample may reflect a problem with the ^{15}N spike concentration in that particular incubation vessel and not necessarily an overnight loss of newly fixed N. The ^{13}C enrichment data do not show the same pattern but rather a leveling off as might be expected during the dark period with perhaps a slight increase upon reentering the light phase at 22 h.

While in *A. oscillarioides* the role of the two cell types can readily be determined by cell morphology, there are important non-heterocystous species of cyanobacteria in which N_2- and CO_2-fixation are integrated in ways that cannot readily be determined by existing methods. The cell-by-cell data presented here show that the diversity of roles and states of individual cells can be inferred from NanoSIMS ^{13}C and ^{15}N enrichment data. In the latter part of the photoperiod, the non-growing, N_2-fixing heterocysts have a wide range of ^{13}C and ^{15}N enrichment (0.05–0.21, 0.22–0.93 APE, respectively), whereas the vegetative cells have much lower variability in ^{13}C and ^{15}N enrichment (0.15 ± 0.01, 0.7 ± 0.02 APE respectively). Although some heterocysts have isotopic enrichment similar to vegetative cells at the 4 and 8 h time steps, most do not. These isotope enrichment patterns, determined for *A. oscillarioides*, provide a useful template against which CO_2- and N_2-fixation in less understood cyanobacteria can be assessed.

In summary, we have demonstrated that isotopic labeling in combination with high-resolution isotopic imaging can be used to characterize temporal and spatial patterns of CO_2- and N_2-fixation and exchange in cells of the filamentous cyanobacterium *A. oscillarioides*. We found rapid export of newly fixed N from heterocysts to vegetative cells and relatively uniform distribution of newly fixed N among vegetative cells, with the exception of those initiating heterocyst differentiation. Features of cell division and relative differences between the biosynthetic age of amino acid C and N used to construct septation walls were also observed. We propose that NanoSIMS analyses, in combination with tracer-level isotope additions, are a useful approach for characterizing CO_2- and N_2-fixation and exchange in *A. oscillarioides* and other cyanobacteria. Subcellular-scale isotopic imaging can also be used to complement studies of gene expression, and in the future, will be particularly important for N metabolism studies. Finally, this approach can be used to study single-cell-level physiological performance in other prokaryotes and material exchanges between adjacent cells, subjects of great importance when studying surface attachment, biofilm formation, biomineralization and cell–cell interactions.

Acknowledgements

We thank Christina Ramon (LLNL) for invaluable assistance in preparing samples for NanoSIMS analysis, Troy Gunderson (USC) for his assistance with the isotope enrichment component of this study and for the IRMS analysis and Larry Nittler (LLNL) for software development. Work was funded in part by the US Department of Energy Office of Biological and Environmental Research Genomics: GTL research program (RP, PKW, JP, SJF, IDH and KHN). Work was performed at LLNL under the auspices of the US Department of Energy under Contract W-7405-Eng-4. DGC also thanks NSF Division of Ocean Sciences for research support.

References

deBoer P, Crossley R, Rothfield L. (1992). The essential bacterial cell-division protein FtsZ is a GTPase. *Nature* **359**: 254–256.

Erickson HP. (1997). FtsZ, a tubulin homologue in prokaryotic cell division. *Trends Cell Biol* **7**: 362–367.

Flores E, Herrero A, Wolk CP, Maldener I. (2006). Is the periplasm continuous in filamentous multicellular cyanobacteria? *Trends Microbiol* **14**: 439–443.

Ghigo J, Beckwith J. (2000). Cell division in *Escherichia coli*: role of FtsL domains in septal localization, function, and oligomerization. *J Bacteriol* **182**: 116–129.

Gotto JW, Tabita FR, Van Baalen C. (1979). Mutants of *Anabaena* strain CA altered in their ability to grow under nitrogen-fixing conditions. *J Bacteriol* **140**: 327–333.

Herrero A, Muro-Pastor AM, Flores E. (1979). Nitrogen control in cyanobacteria. *J Bacteriol* **183**: 411–425.

Klint J, Rasmussen U, Bergman B. (2007). FtsZ may have dual roles in the filamentous cyanobacteria Nostoc/Anabaena sp. strain PCC 7120. *J Plant Physiol* **164**: 11–18.

Kumar A, Tabita FR, Van Baalen C. (1983). High endogenous nitrogenase activity in isolated heterocysts of *Anabaena* sp. strain CA after nitrogen starvation. *J Bacteriol* **155**: 493–497.

Lechene C, Hillion F, McMahon G, Benson D, Kleinfeld AM, Kampf JP *et al.* (2006). High-resolution quantitative imaging of mammalian and bacterial cells using stable isotope mass spectrometry. *J Biol* **5**: 20.

Mazouni K, Domain F, Cassier-Chauvat C, Chauvat F. (2004). Molecular analysis of the key cytokinetic components of cyanobacteria: FtsZ, ZipN and MinCDE. *Mol Microbiol* **52**: 1145–1158.

Meeks JC, Elhai J. (2002). Regulation of cellular differentiation in filamentous cyanobacteria in free living plants and plant-associated symbiotic growth states. *Microbiol Mol Biol Rev* **66**: 94–121.

Meeks JC, Wolk CP, Thomas J, Lockau W, Shaffer PW, Austin SM *et al.* (1977). The pathways of assimilation of $^{13}NH_4^+$ by the cyanobacterium *Anabaena cylindrica*. *J Biol Chem* **252**: 7894–7900.

Murry MA, Hallenbeck PC, Benemann JR. (1984). Immunochemical evidence that nitrogenase is restricted to the heterocysts in *Anabaena cylindrica Arch. Microbiology* **137**: 194–199.

Simon RD. (1987). Inclusion bodies in the cyanobacteria: cyanophycin, polyphosphate, polyhedral bodies. In: Fay P, Van Baalen C (eds). *The Cyanobacteria*. Elsevier: Amsterdam, pp 199–225.

Smith RL, Van Baalen C, Tabita FR. (1987). Alteration of the Fe protein of nitrogenase by oxygen in the cyanobacteium *Anabaena sp.* strain CA. *J Bacteriol* **169**: 2537–2542.

Stewart WDP. (1973). Nitrogen fixation by photosynthetic microorganisms. *Annu Rev Microbiol* **27**: 283–316.

Thomas J, Meeks JC, Wolk CP, Shaffer PW, Austin SM. (1977). Formation of glutamine from [^{13}N] ammonia, [^{13}N] dinitrogen, and [^{14}C] glutamate by heterocysts isolated from *Anabaena cylindrica*. *J Bacteriol* **129**: 1545–1555.

Thomas J, Wolk CP, Shaffer PW, Austin SM, Galonsky A. (1975). The initial organic products of fixation of ^{13}N-labeled nitrogen gas by the blue-green alga *Anabaena cylindrica*. *Biochem Biophys Res Commun* **67**: 501–507.

Walsby A. (1972). Structure and function of gas vacuoles. *Bacteriol Rev* **36**: 1–32.

Wolk CP. (1968). Movement of carbon from vegetative cells to heterocysts in *Anabaena cylindrica*. *J Bacteriol* **96**: 2138–2143.

Wolk CP. (1996). Heterocyst formation. *Annu Rev Genet* **30**: 59–78.

Wolk CP. (2000). Heterocyst formation in *Anabaena*. In: Brun YV, Shimkets LJ (eds). *Prokaryotic Development*. Amer Soc Microbiol Press: Washington, DC, pp 83–104.

Wolk CP, Thomas J, Shaffer PW, Austin SM, Galonsky A. (1976). Pathway of nitrogen metabolism after fixation of ^{13}N-labeled nitrogen gas by the cyanobacterium *Anabaena cylindrica*. *J Biol Chem* **251**: 5027–5034.

Wolk CP, Austin SM, Bortins J, Galonsky A. (1974). Autoradiographic localization of ^{13}N after fixation of ^{13}N-labeled nitrogen gas by a heterocyst-forming blue-green alga. *J Cell Biol* **61**: 440–453.